

insertion devices is 2.5 m. The schematic layout of the different components in one of the long straight sections, along with an insertion device is shown in Fig. 1.

In the first phase of Indus-2 insertion device installation, two out-vacuum pure permanent magnet (ppm) linear undulators will be installed. The first linear undulator U-1, is designed for the Atomic Molecular and Optical Sciences (AMOS) beam line to generate photons with a maximum flux between 6 eV and 250 eV [1] (Fig. 2(a)) while the second linear undulator U-2 is designed for the Angle Resolved and Angle Integrated Photoemission Spectroscopy (ARPES) beam line to generate photons with a maximum flux between 30 eV and 600 eV (Fig. 2(b)). The technical parameters of the

Indus-2 storage ring and linear undulators U1 and U2 are given in Table 1 and Table 2 respectively.

Table 1. Indus-2 storage ring parameters.

electron energy/GeV	2.5	
beam current/mA	300	
coupling constant ($\varepsilon_y/\varepsilon_x$)	1%	
emittances ($\varepsilon_x, \varepsilon_y$)	58 nm-rad	0.58 nm-rad
*betatron parameter (β_x, β_y)	14.02 m	2.01 m
*electron beam size (σ_x, σ_y)	903 μm	34 μm
*electron beam divergence (σ'_x, σ'_y)	64 μrad	17 μrad
* η_x, η_y	0	0
* η'_x, η'_y	0	0
natural energy spread	9.03258e-4	

*Given values are at the centre of the undulator

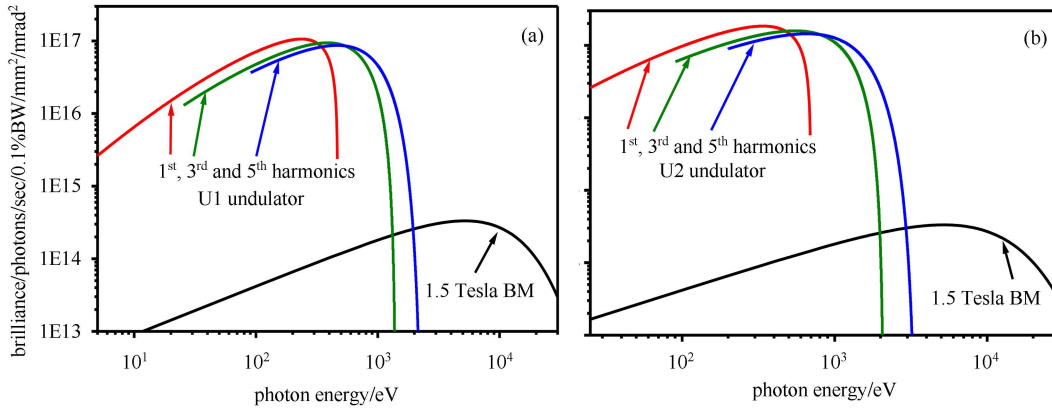


Fig. 2. (color online) Brilliance from (a) U1 and (b) U2 undulator.

Table 2. Parameters of Indus-2 insertion devices

insertion device	beam lines	magnetic field B/T , period length, λ/mm , number of periods(n)	total length/m	operating photon energy range/eV
undulator U1	Atomic Molecular and Optical Sciences (AMOS) beam line	$B_y=1.06, \lambda=126, n=18$	2.5	6–250
undulator U2	Angle Resolved and Angle Integrated Photoemission Spectroscopy (ARPES) beam line	$B_y=0.86, \lambda=85, n=26$	2.5	30–600

2 Effect of undulators on Indus-2 beam parameters

The magnetic fields of Insertion Devices (IDs) introduce perturbations to the circulating electron beam and hence affect the linear and nonlinear beam dynamics of the electron beam in a storage ring. Studying the effect of IDs is essential for two purposes: first, to avoid degradation in the performance of the storage ring and second, to avoid any variation in the synchrotron radiation photon beam characteristics, which are primarily defined by the electron beam parameters of the radiation source point. In this section the effect of the linear undulators U1 and U2 are explored at 2.5 GeV.

2.1 Effect on betatron tune

The electron beam inside a linear undulator follows a wiggling trajectory, which crosses the vertical magnetic field at an angle between the poles. Vertically off-axis, there is a longitudinal magnetic field B_s that couples the angular deflection of the beam in the horizontal plane to give a position-dependent force which always acts towards the beam axis [2]. This is an intrinsic focusing effect generated by an ideal linear undulator and is treated as a second order effect, being proportional to the square of the field and inversely proportional to the square of the energy. Along with the intrinsic effect of the undulator, the manufacturing tolerances and field roll-off due to finite magnet pole width also contribute to the tune

variation. The tune variation due to insertion devices can be calculated using kick maps, generated by the RADIA software developed at the European Synchrotron Radiation Facility (ESRF) [3]. The kick map is basically the space dependent kicks [4], defined as

$$x' = -\frac{\alpha^2}{2} \int_{-\infty}^{\infty} \frac{\partial \Phi(x, z, s)}{\partial x} ds + o(\alpha^3), \quad (1)$$

and

$$z' = -\frac{\alpha^2}{2} \int_{-\infty}^{\infty} \frac{\partial \Phi(x, z, s)}{\partial z} ds + o(\alpha^3), \quad (2)$$

where

$$\Phi(x, z, s) = \left(\int_{-\infty}^{\infty} B_x ds \right)^2 + \left(\int_{-\infty}^{\infty} B_z ds \right)^2,$$

and

$$\alpha = \frac{e}{\gamma mc}.$$

Here e is the charge of the electron, γ is the relativistic factor, m is the rest mass of the electron and c is the speed of light in a vacuum, x and z are the horizontal and vertical dimension respectively. The variation of angular kicks (Eqs. (1) & (2)) in space gives the focusing effect due to the insertion device. Using the kick map in the Accelerator Tool (AT) box simulation code, the tune variation due to undulators U1 and U2 are calculated. The tune variation in the vertical plane is 0.0063 and 0.0036 for the undulators U1 and U2, respectively. Variations in tune due to both the undulators are considerable in magnitude and hence need to be corrected to avoid any detrimental effect of resonance in the machine.

2.2 Effect on betatron amplitude function

The additional focusing effect described in Section 2.1 causes the betatron amplitude function to change (beta-beat), which leads to breaking the periodicity of the machine optics. Breaking of lattice periodicity by insertion devices may be inevitable, and nonlinearities present in the lattice may yield a significant reduction in the dynamic aperture and hence in lifetime. Moreover, distortion in beta functions causes a change in the beam sizes and hence also affects the properties of the synchrotron radiation. The maximum distortion in the beta function due to the insertion devices can be given by the following relation [5]:

$$\left[\frac{\Delta \beta_y}{\beta_y} \right]_{\max} = \frac{\beta_y^{\text{avg}} L_{\text{id}}}{4\rho_{\text{id}}^2 \sin(2\pi Q_y)}, \quad (3)$$

where β_y^{avg} is the average vertical beta function over the length of the undulator; $\rho_{\text{id}}(\text{m}) = (10/3) \times (E/B_0)$; E is the energy of the electron beam (GeV); B_0 is the peak magnetic field of the undulator (T); L_{id} is the length of the undulator; and Q_y is the vertical betatron tune value.

Betabeat for the maximum field/lowest gap of undulators U1 and U2 are shown in Fig. 5. The maximum

beta variation due to both insertion devices is less than 7% and, taking the change in emittance into account, the maximum beam size variation in the Indus-2 ring is less than 10%. Hence, from the synchrotron radiation user point of view, there is no need for beta-beat correction in the ring, though it may be required to counter its influence on the machine beam dynamics via the symmetry breaking and non-linear effects mentioned above. In the next section, a scheme of beta-beat and tune compensation is proposed to mitigate the effect of non-linearities in the lattice. This also ensures a better beam size stability for the synchrotron radiation beam line users.

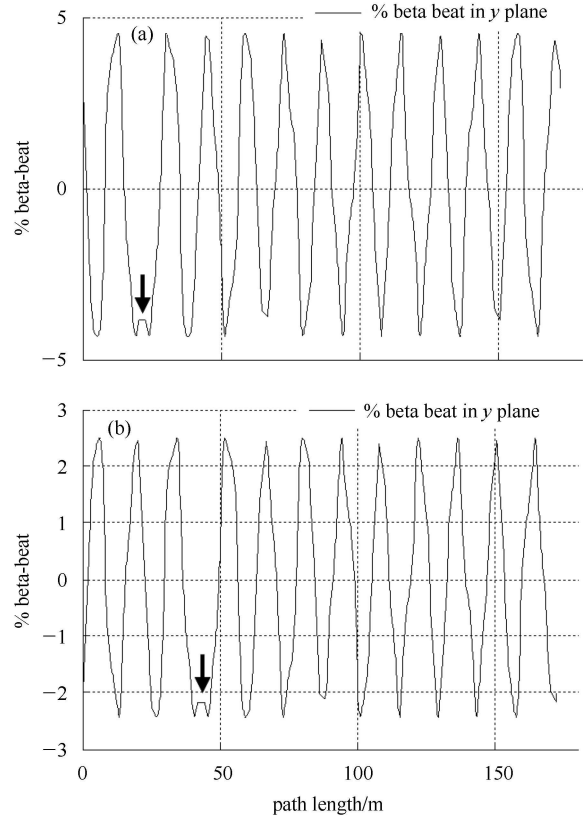


Fig. 3. Beta-beat due to (a) undulator U1 and (b) undulator U2. The arrow shows the location of the undulator.

2.3 Compensation of betatron tune and beta-beat

In Indus-2, a total of five families of quadrupoles, namely Q1D, Q2F, Q3D, Q4F and Q5D, are employed in each super-period. A pair of quadrupole magnets for each of the Q1D, Q2F and Q3D families is placed in the long straight section, while two quadrupoles for the Q4F family and one quadrupole for the Q5D family are placed in the short straight section (shown in Fig. 4). Each pair of quadrupole magnets in a long straight section is powered by a single power supply, while Q4F and Q5D

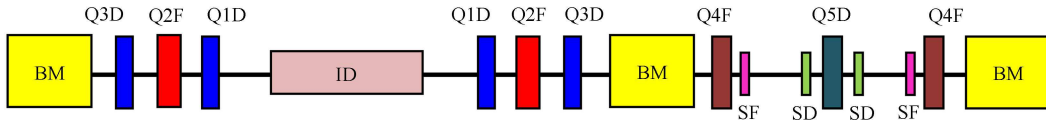


Fig. 4. (color online) Quadrupole distribution around ID/undulator in Indus-2.

family quadrupoles of all the short straight sections are powered by two power supplies, one for each family. The beta-beat generated due to undulators in Indus-2 is corrected by restoring the betatron amplitude function in both the planes just at the entry and exit of the upstream and downstream quadrupoles Q2F respectively. Since the lattice is symmetric, alpha is automatically corrected as a result. This is known as the alpha matching technique. Here, the source of perturbation is the undulator, and the nearby quadrupoles, i.e. the two Q1D quadrupoles and the two Q2F quadrupoles adjacent to the undulator, are very effective in restoring the beta functions in both planes. The remaining Q2F family quadrupoles in the rest of the long straight sections and the Q3D family quadrupoles of all the straight sections are used for the tune correction.

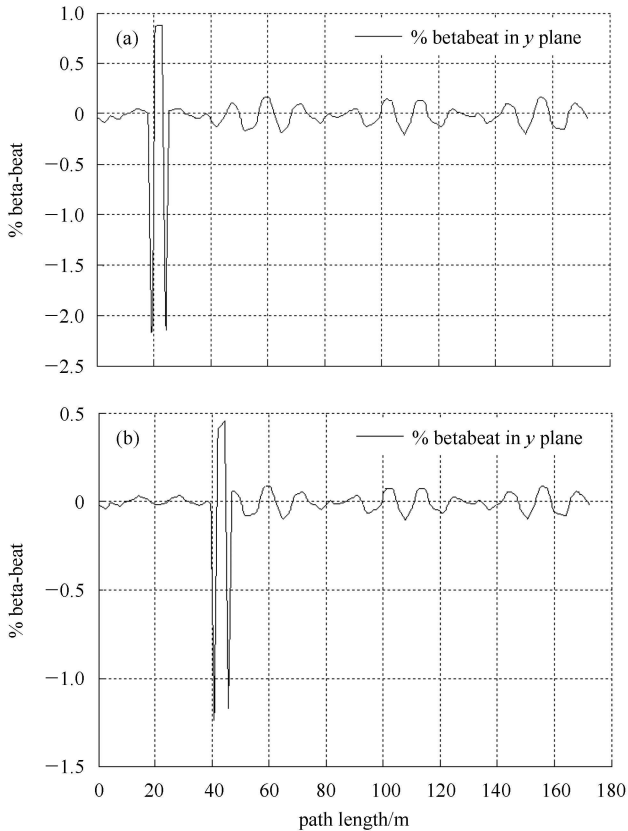


Fig. 5. Alpha matching using local quadrupoles of Q1D and Q2F family around (a) undulator U1 and (b) undulator U2. Tune correction is done with the remaining quadrupoles from the Q2F and Q3D families.

In Fig. 5(a) and Fig. 5(b), the plots after the beta-beat correction are shown, while the strength change required for beta-beat compensation is presented in Table 3. The strength change required for the tune compensation is very small (percentage change of 10^{-2}).

Table 3. Quadrupole strength for beta-beat compensation.

undulator	beta-beat	percentage change in quadrupole strength for beta-beat correction (local Q1D and Q2F quadrupoles)
U1	$\pm 4.3\%$	$[-5.5 \ -1.2]$
U2	$\pm 2.5\%$	$[-3 \ -0.77]$

2.4 Effect on closed orbit

Two important requirements for experiments at insertion device beam lines are that the operation of a given ID is transparent to other beamline users, and that the photon beam remains stable for all operating pole gaps adjustment of undulators. In the magnetic optimization of IDs undertaken in the laboratory, every effort is made to achieve a straight trajectory inside the ID with minimal phase errors; still there exist nonzero first and second magnetic field integrals, which also vary with the ID pole gaps. Nonzero integrated dipole fields of an insertion device deflect the electron beam inside the insertion device. This results in a closed-orbit displacement of the stored electron beam over the entire ring. In addition, if the electron beam is placed somewhere off-center in the insertion device, the integrated-quadrupole error looks like a dipole and steers the beam [6–8]. This results in a closed-orbit distortion that can be larger than the acceptable limit. Therefore, to control the orbit distortion in both planes, there is a plan to install two pairs of correctors (one pair for correction in each plane) at both edges of the undulator. In our simulation, the strengths of the correctors have been calculated using the orbit response matrix. Let the orbit response matrix be denoted by R , which is an $M \times N$ matrix. M and N are the numbers of BPMs and corrector magnets respectively. The element R_{ij} of the orbit response matrix corresponds to the orbit shift at the i^{th} BPM due to a unit kick from the j^{th} corrector and is given by

$$R_{ij} = \frac{\sqrt{\beta_i \beta_j}}{2 \sin(\pi Q)} \cos(|\varphi_i - \varphi_j| - \pi Q), \quad (4)$$

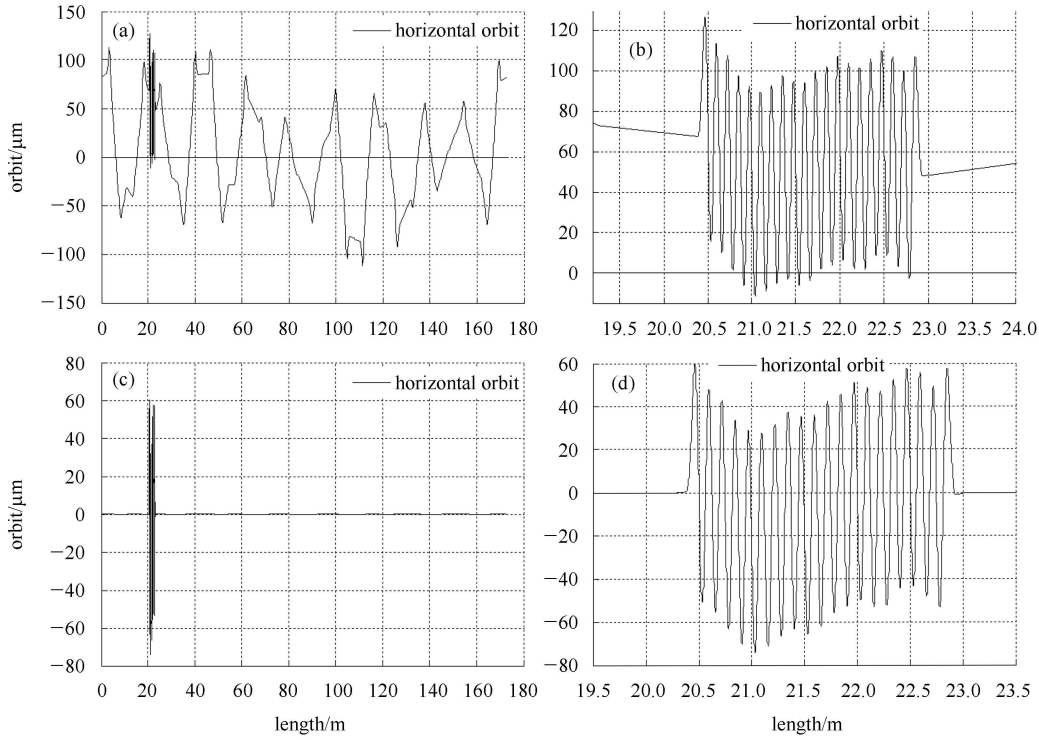


Fig. 6. (a) Horizontal orbit due to random errors in peak field of undulator. (b) Electron beam trajectory in the undulator in the presence of random errors in the peak field. (c) Horizontal orbit after orbit correction using two correctors around the undulator (d) Electron beam trajectory in the undulator after orbit correction.

where (β_i, φ_i) , and (β_j, φ_j) are the beta function and phase advance at the BPM and corrector magnet locations, and Q is the betatron tune.

The strength of the correctors can be found by the following relation

$$\theta = R^{-1}y. \quad (5)$$

Here θ is the vector for the strength of the correctors and y is the vector of orbit deviations due to the undulator. In Fig. 6(a) the orbit distortion throughout the ring due to the random errors in the peak magnetic field of the undulator is shown. The random errors in the peak magnetic field, having first dipole field integrals of nearly ~ 100 G-cm (nearly double the defined tolerance) generate the maximum horizontal orbit distortion of ~ 110 microns in the ring. In Fig. 6(b), the trajectory inside the undulator is shown. It is displaced ~ 72 microns away from the normal trajectory, which in turn displaces the synchrotron radiation source used by the beam line user. In Fig. 6(c) and Fig. 6(d), the trajectories of the electron beam throughout the ring and inside the undulator are shown after orbit compensation using two correctors. The total strengths of the correctors required for the horizontal orbit compensation are ~ 100 G-cm. Similarly the required strength of the correctors in the vertical plane is ~ 50 G-cm for compensation of vertical orbit distortion.

2.5 Effect on emittance

The brightness of the photon beam depends on the electron beam emittance of the storage ring. In a storage ring, the emittance is basically decided by the equilibrium between quantum fluctuations and the synchrotron radiation damping process. The emittance in a ring is given by the following expression:

$$\epsilon_x^0 = C_q \gamma^2 \frac{I_5}{I_2 - I_4}, \quad (6)$$

where γ is the relativistic factor, $C_q = 3.83 \times 10^{-13}$ m, $I_2 = \oint \frac{1}{\rho^2} ds$, $I_4 = \oint \frac{\eta}{\rho} \left(\frac{1}{\rho^2} + 2k_1 \right) ds$ and $I_5 = \oint \frac{H}{|\rho|^3} ds$. Here, $H = \gamma\eta^2 + 2\alpha\eta\eta' + \beta\eta'^2$, $\alpha = -\frac{1}{2} \frac{d\beta}{ds}$, η is dispersion, η' is the derivative of η w.r.t. s , k_1 is the field index, and $\beta\gamma - 1 = \alpha^2$. I_2 , I_4 and I_5 are the synchrotron integrals. The presence of the undulator in the ring makes the synchrotron integrals change and hence there will be a change in emittance of the ring. Taking the effect of the undulator into account, Eq. (6) can be written in the following manner [7]:

$$\epsilon_x = \epsilon_x^0 \frac{1 + \frac{\Delta I_5}{I_5^0}}{1 + \frac{\Delta I_2 - \Delta I_4}{I_2^0 - I_4^0}}. \quad (7)$$

The superscript 0 denotes the value evaluated without considering the effect of the undulator. In Indus-2, with the designed optics, the dispersion functions in the long straight section, where the undulator will be installed, are almost zero and moreover the contribution of the undulator itself to the dispersion functions is very small. Therefore, for the designed optics of Indus-2, the synchrotron radiation damping effect will dominate over the quantum fluctuation and this will lead in turn to a reduction of the electron beam emittance. The reduction in emittance at 2.5 GeV beam energy due to undulators U1 and U2 is 1.74% and 1.1% respectively.

2.6 Effect on energy spread

The equilibrium energy spread of the electron beam in the storage ring is also determined by two phenomena, the statistical emission of photons in the form of synchrotron radiation (SR) and the damping effect due to SR emission. The energy spread of a storage ring is given by the following relation

$$\sigma_E^0 = \left[E \left(C_q \gamma^2 \frac{I_3}{2I_2 + I_4} \right)^{1/2} \right], \quad (8)$$

where the synchrotron integral $I_3 = \oint \frac{1}{|\rho|^3} ds$. For separate

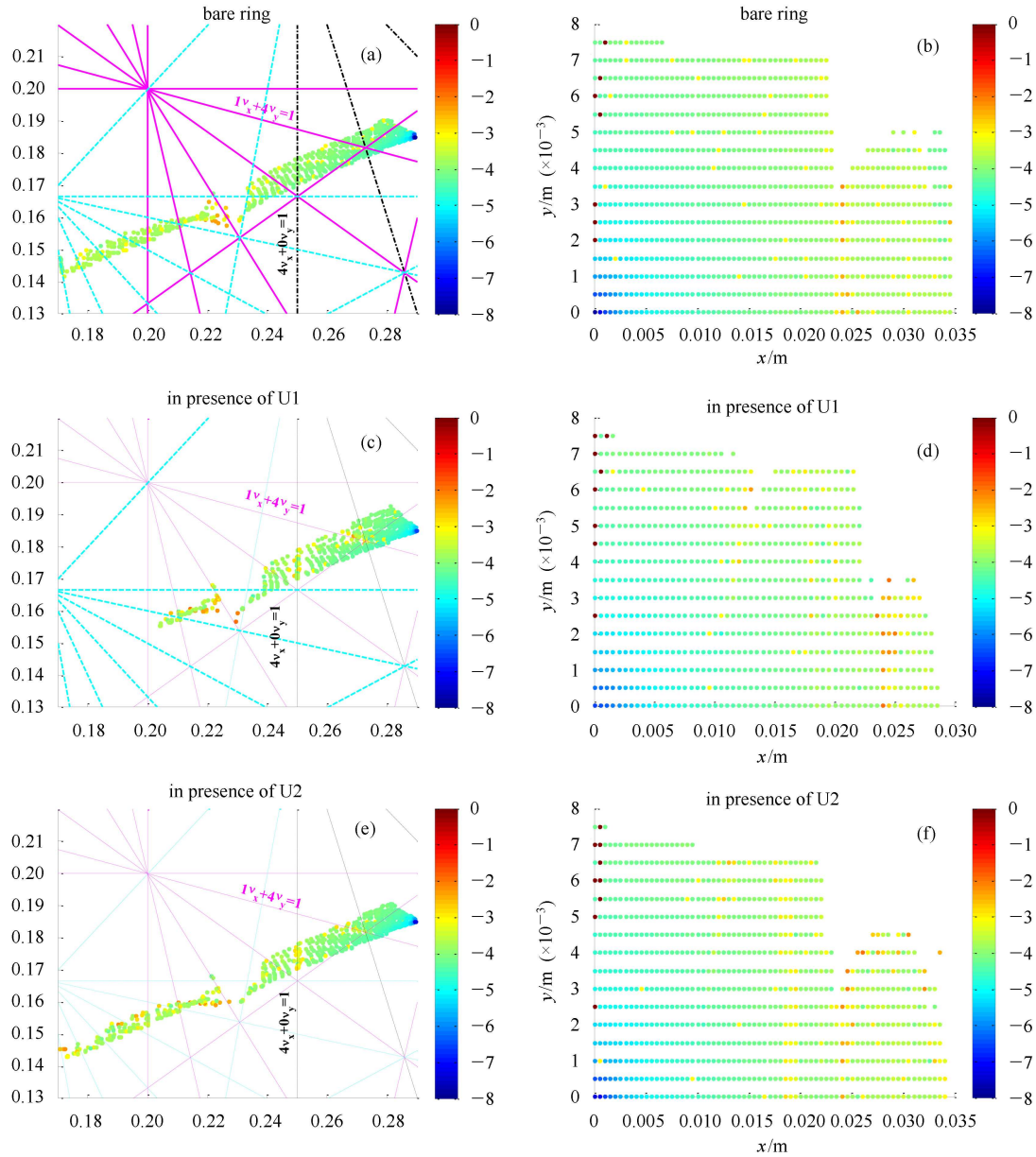


Fig. 7. (color online) Frequency map analysis of bare ring and with undulators U1 and U2.

function lattices, I_4 is much smaller than I_2 and hence we can neglect it. The energy spread of a storage ring is affected by the presence of an undulator. From Eq. (8), the energy spread in the presence of an undulator is given by [9]:

$$\sigma_E = \sigma_E^0 \left[\frac{1 + \Delta I_3 / I_3^0}{\Delta I_2 / I_2^0} \right]^{1/2}. \quad (9)$$

The superscript 0 denotes that the value is evaluated without considering the effect of the undulator. The calculations have been carried out for energy spread variation and show a reduction of 0.36% and 0.3% at the minimum gap of undulators U1 and U2 respectively in the Indus-2 ring.

2.7 Nonlinear effects of undulators

Frequency map analysis (FMA) is a possible way to obtain an understanding of the resonances affecting the dynamic aperture and of the nonlinear characteristics in the presence of insertion devices. It is a very efficient technique for understanding the resonances, which may affect the stability of the electrons. In the FMA simulation [10, 11], particles are tracked for 2048 turns and for the surviving particles the transverse tunes (v_x^1, v_y^1) and (v_x^2, v_y^2) are computed over two consecutive samples of 1024 turns. The diffusion rate D is then calculated as

$$D = \log_{10} \sqrt{[(v_x^1 - v_x^2)^2 + (v_y^1 - v_y^2)^2]}.$$

The diffusion rate is coded by a color scale from blue for stable motion to red for unstable and chaotic motion (color online). In Fig. 7(a), Fig. 7(c) and Fig. 7(e) the tune diffusion coefficients are plotted with horizontal and vertical tune for the bare lattice, lattice with the presence of undulator U1 and lattice with the presence of undulator U2 respectively. In Fig. 7(b), Fig. 7(d) and

Fig. 7(f), the tune diffusion coefficients are plotted with the transverse positions x and y for the bare lattice, the lattice with the presence of undulator U1 and the lattice with the presence of undulator U2 respectively. FMA with the presence of undulators reveals that the aperture available to the beam is mainly restricted by the small vertical aperture of the undulator vacuum chamber. In Figs. 7(d) and 7(f), a very small dip in dynamic aperture can be seen at $x \sim 13-15$ mm, due to the presence of undulators U1 and U2 respectively. The reduction in dynamic aperture is mainly due to the 5th order sum resonance line $v_x + 4v_y = 1$. The jaws of the undulators will be completely open at the injection energy (550 MeV), so the injection efficiency will not be affected, while at 2.5 GeV, a sufficiently damped beam has enough room up to $x = \pm 15$ mm and hence the lifetime will also not be affected.

3 Conclusion

We investigated the effects of two plane polarized undulators on the stored beam of Indus-2. With either of the linear undulators present, there is variation in betatron tune and betatron amplitude, for which a compensation scheme is also discussed. Due to the dominating effect of radiation damping with the presence of the undulators, the emittance and energy spread of the Indus-2 electron beam are reduced and are within the specified limits for the synchrotron radiation users. Moreover, the FMA reveals that the nonlinear effect of the undulators will not affect the performance of the storage ring.

We would like to thank Shri S. Das for providing the brilliance curves of the undulators and Shri D. P. Yadav for providing the layout of Indus-2 long straight section.

References

- 1 Das A K, Raja Sekhar B N, Jagatap B N et al. Radiation characteristics of a Planar Permanent Magnet (PPM) Undulator for Atomic Molecular & Optical Science (AMOS) beamline. Proc. of InPAC. 2013. 302–304
- 2 Walker R P. Wigglers. CERN Accelerator School: 5th Advanced Accelerator Physics Course. CERN-95-06, 807–835
- 3 <http://www.esrf.eu/Accelerators/Groups/InsertionDevices/Software/Radia/Examples>
- 4 Elleaume P. A New Approach to the Electron Beam Dynamics in Undulators and Wigglers. Proc. of EPAC. 1992. 661
- 5 Kim Eun-San. Journal of the Korean Physical Society, 2005, **46**(5): 1125–1130
- 6 Kincaid B M. Nucl. Instrum. Methods Phys. Res., Sect. A, 1990, **291**(1–2): 363–370
- 7 Rugmai S. ScienceAsia, 2005, **31**: 159–165
- 8 Dasri T, Rugmai S. Walailak J Sci. & Tech., 2012, **9**(1): 83–92
- 9 Chao H C, Kuo C C. Beam Dynamics Effects with Insertion Devices for the Proposed 3 GeV Ring in Taiwan. Proc. of APAC. 2007. 196–198
- 10 Nadolski L, Laskar J. Phys. Rev. ST Accel. Beams, 2003, **6**: 114801
- 11 Steier C, Wan W. Quantitative Lattice Optimization Using Frequency Map Analysis. Proc. of IPAC. 2010. 4746–4748